Signal Processing for Smart Sensors

Franco Maloberti, Valentino Liberali and Piero Malcovati

Integrated Microsystems Laboratory, University of Pavia
Via Ferrata 1, 27100 Pavia, Italy
Tel. +39 382 505205, Fax. +39 382 505677
E-Mail: franco@ele.unipv.it, valent@ele.unipv.it, piero@ele.unipv.it

Abstract

Future integrated systems will benefit significantly from the progress in batch-manufactured silicon sensors and signal processing techniques. This paper presents various design examples to illustrate specific problems and solutions associated with front-end electronics, data converters and signal processing functions for smart sensors.

1. Introduction

Smart sensors include on the same micro-module the sensing element and the interface circuit, in order to perform a suitable processing of the sensor signals before the transmission to the rest of the system [1, 2, 3]. We can distinguish between sensors that can be fabricated directly on the silicon substrate used for the integrated circuits and sensors that have to be assembled together with the interface circuit in a multi-chip module. Both approaches allow batch manufacturing of either the integrated circuit and the sensing elements. Consequently, cost effective microsystems including sensors, circuits and eventually actuators can be fabricated, opening new perspective markets. Challenges arise from the technology, the level of the sensor signals, the packaging requirements, the testing of physical-electrical (or chemical-electrical) systems, the aggressive environment and even the signal processing functions required. Smart sensors, indeed, typically require specific signal processing functions to match the characteristics of both sensor and system.
This paper presents our recent activity in the field of signal processing for smart sensors. Various design examples are reported to illustrate specific problems and solutions associated with front-end electronics, data converters and signal processing functions for smart sensors.

2. Front-End Circuits

A common problem of sensor systems is the low level of the electrical signals available at the output of the sensing element. Handling low-level signals is not unusual in electronics, but specific sensors typically introduce additional constraints which require dedicated solutions. The two examples discussed below show how we handled the issue.

Continuous Time Circuits (UV Sensor)

The output current delivered by photo-diodes with enhanced ultraviolet (UV) responsivity is in most cases very small, thus requiring an interface circuit with very large current gain [4]. An integrated UV sensor consists of very shallow *p* and *n* implantations, which create a depletion region very close to the crystal surface where UV light can penetrate and generate carriers. Although the thickness of the implantations is not standard, adding a few additional steps to the a standard process allows the sensors to be realized and on-chip circuitry to be integrated.

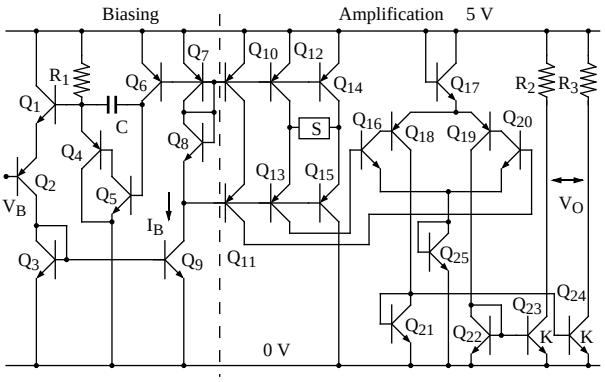

Fig. 1. Schematic of the UV diode readout circuit

The current generated by the UV diode ranges from 10 pA to 1 nA). Therefore, large current gain and low noise are the most important requirements for the readout circuit. Bipolar transistors are, therefore, better suited than CMOS for this application because of their lower flicker noise and larger transconductance-to-current ratio. Moreover, since the system does not require very accurate control of the current gain, we can exploit the bipolar transistor current gain β to amplify the signal current and use a resistor to obtain an output voltage.
The schematic of the bipolar transimpedance amplifier realized for this application [5] is shown in Fig. 1. The UV diode (*S*) current and the bias current (I_B) are amplified by Q_{16} and Q_{18}. Moreover, a replica of I_B is amplified by Q_{19} and Q_{20}.The resulting currents, properly mirrored (Q_{21}, Q_{22}, Q_{23} and Q_{24}), are transformed into voltages by R_3 and R_2. The left part of the circuit generates a suitable DC bias current, by means of a feedback loop. Voltage V_B allows to control I_B in the range 5 to 15 nA.

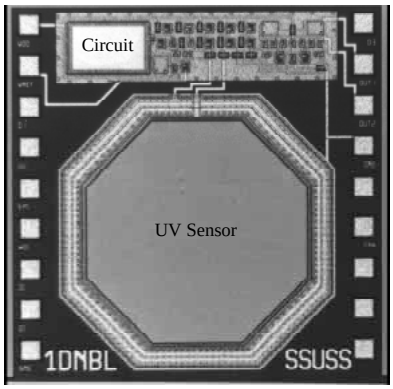

Fig. 2. Microphotograph of a silicon UV diode

Assuming perfect element matching, the output voltage of the circuit V_O can be expressed as a function of the diode current I_D,

$$V_O = \beta_{16}\beta_{18}KR_3I_D. \quad (1)$$

With β around 200, R_3 = 20 kΩ and a mirror factor K equal to 2, a transresistance gain of 10^9 Ω can be achieved.
The transimpedance amplifier was integrated together with a UV diode in a modified bipolar process. Fig. 2 shows a microphotograph of the chip, while Fig. 3 shows the measured output voltage of the system as a function of the UV diode current. The obtained transimpedance is, as expected, 10^9 V / A.

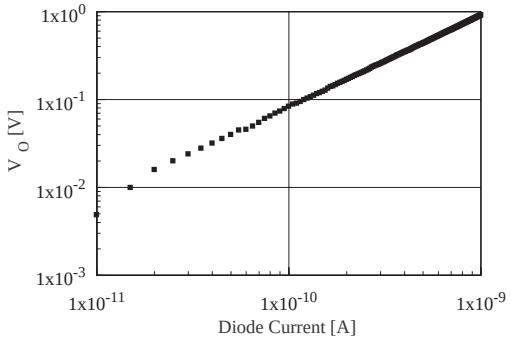

Fig. 3. Measured output voltage of the UV detector

Sampled Data Circuits (Thermoelectric IR Sensor)

Bulk micromachining allows us to realize thermally insulated membranes, as shown in Fig. 4. A selected part of a chip can hence be heated by an external infrared radiation (IR) flow. Thermal insulation means that the temperature of the membrane rises in comparison with the silicon bulk and the temperature difference achieved gives a measure of the IR flow [6].
A convenient device for on-chip temperature detection is the thermopile. The thermopile is the series connection of a large number of thermocouples consisting of poly1 (*n*-doped) and poly2 (*p*-doped) lines. The signal resulting from a small IR flow (for example emitted by the human body) is in the μV range. Therefore, the task of the electronic interface is difficult, since the circuitry has to provide very low noise and low offset amplification. This difficult target can be achieved in CMOS technology by assuming the signal bandwidth to be fairly low [7]. The use of the autozero technique and the successive low frequency filtering of outband noise components allows us to achieve the required sensitivity. Fig. 5 shows the input stage of the sensor interface. It is a four-input transconductance stage, where two inputs of the transconductor are used for the signal amplification and two for the autozero operation. During the autozero phase, the transconductor is buffer-connected. Therefore, the offset and low frequency noise are measured and stored in the autozero capacitors (C_{az}). During the measurement phase the stored voltage is subtracted from the signal, giving rise to a clean output current. This current is integrated over a large number of clock periods on the capacitor of the following stage to perform the required low-pass filtering.

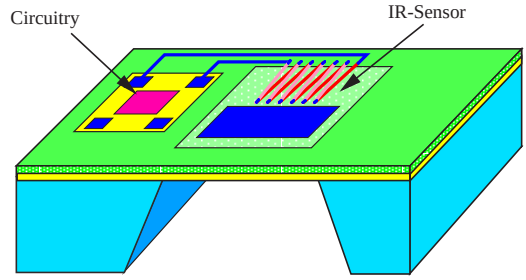

Fig. 4. Microsystem for IR sensing

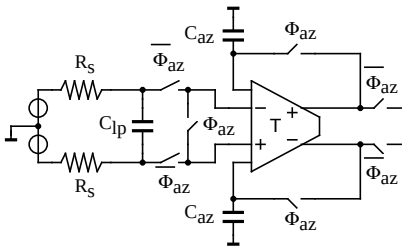

Fig. 5. Autozeroed preamplifier for the IR sensor

A microphotograph of the infrared microsystem chip is shown in Fig. 6. To ensure the maximum testing flexibility, the sensors are not directly connected to the readout circuitry, but some pad openings are available for local bonding.

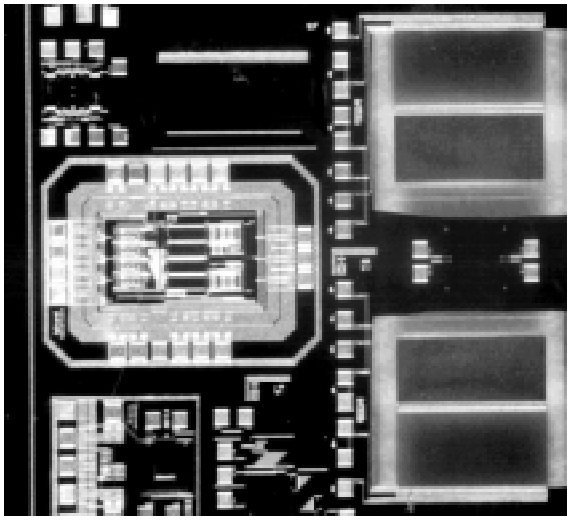

Fig. 6. Microphotograph of the IR microsystem chip

Fig. 7 shows the output signal (waveform 1) obtained by focusing chopped infrared radiation on the sensor (waveform 2 is the 3 Hz chopping signal). The power density of the radiation is 2 µW/mm^2 (corresponding to a temperature difference of 3 K), and the active area of the sensor is 0.84 mm^2. The total power collected is therefore 1.68 µW. In this case the gain of the amplifier is 75 dB. We can observe that the noise level is well below the signal level.

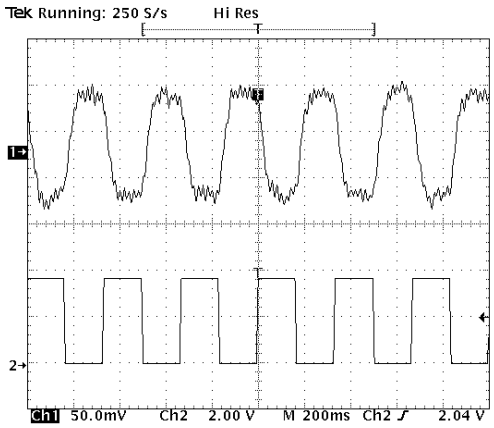

Fig. 7. Measured response of the IR microsystem to a 3 Hz, 1.68 µW chopped infrared waveform

3. A/D Converters

In sensor systems, after the preliminary signal conditioning performed by the front-end circuitry, it is typically necessary to convert the signals into the digital domain. This section discusses some practical implementations of analog-to-digital converters for sensor systems based on various conversion techniques. In view of the narrow bandwidth of most physical or chemical signals oversampled A/D converters (incremental ADCs and sigma-delta modulators) are typically used in sensor systems, since they allow high resolutions to be achieved without precise analog component. However, when low power consumption and fast conversion time are required, for example in portable or battery operated devices, successive approximation ADCs (or in general Nyquist rate A/D converters) are widely used.

Incremental ADC (2D Magnetic Sensor)

Magnetic sensors are generally compatible with standard IC technologies and are widely used in several applications. Among them we will consider the 2D magnetic sensor system for angular measurements (vector probe), whose block diagram of is shown in Fig. 8 [8].

Two orthogonal pairs of magnetic sensors (Hall devices) together with the front-end circuitry deliver two differential voltages proportional to the *X* and *Y* components of the magnetic field produced by a permanent magnet placed on top of the chip. The sensor geometry and the readout circuit have been optimized to reduce offset and temperature effects, as well as to relax as much as possible the mechanical tolerances of the system. Since the resulting front-end output voltages are in the order of few tens of mV only, a couple of instrumentation amplifiers (Fig. 9) is required to achieve a reasonably large signal level at the input of the subsequent A/D converter.

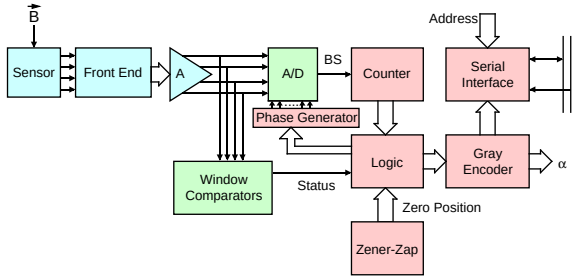

Fig. 8. Block diagram of the rotary switch interface circuit

Indeed, the differential output voltages of the instrumentation amplifier $V_{X1} - V_{X2}$ and $V_{Y1} - V_{Y2}$ represent alternatively the input or the reference signal of an incremental A/D converter (Fig. 9), depending on the quadrant of the magnetic field angle *Q* (actually, the input clock phases are varied depending on *Q*). The correct value of *Q* is determined by a finite state machine in the digital section, as shown in Fig. 10.

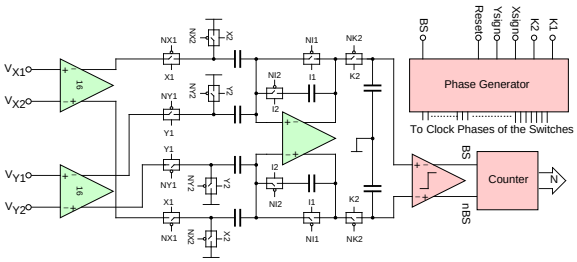

Fig. 9. Schematic of the incremental A/D converter

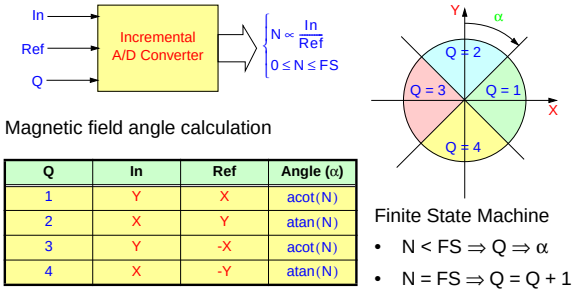

Fig. 10. Operating principle of the incremental A/D converter

Once the quadrant is determined, the bitstream delivered by the A/D converter is decimated by a counter, producing an output word *N* proportional to the ratio between the magnetic field components. Finally, a look-up table transforms *N* into the magnetic field angle using a Gray code representation.

In order to avoid abnormal operation of the vector probe due to the absence of the permanent magnet, we included in the system two window comparators (threshold ±100 mV), which check the magnetic field strength and deliver to the digital section a suitable status bit.

The microphotograph of the chip is shown in Fig. 11, while Fig. 12 shows the measured output digital word as a function of the magnetic field angle.

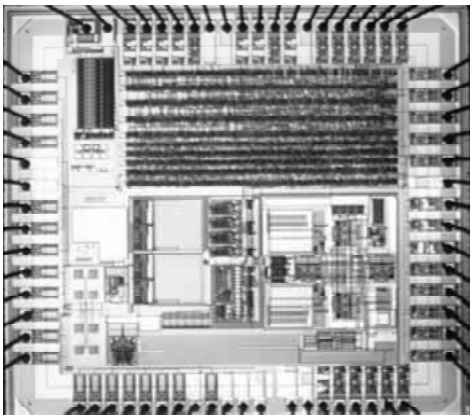

Fig. 11. Microphotograph of the 2D magnetic sensor system

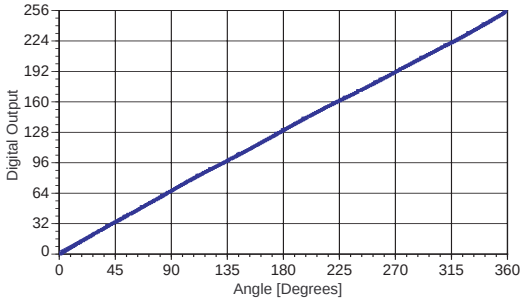

Fig. 12. Measured output digital word as a function of the magnetic field angle

Successive Approximation ADC (3D Magnetic Sensor)

Several working environments, such as hospitals (magnetic resonance) or physics laboratories (nuclear experiments) are polluted by strong low-frequency magnetic fields. In order to guarantee the workers' health, therefore, it is essential to monitor the exact integral exposure of each worker to a particular level of field.

The level of magnetic field which is known to be dangerous for human beings can be detected by silicon magnetic sensors fabricated in conventional CMOS technologies. However, the bias current required to achieve the desired sensitivity (a few mA) is too high to allow battery operation. This potential drawback is circumvented by choosing a particular architecture for the A/D interface, which allows pulsed operation of the sensor with a very small duty cycle. Therefore, in spite of the large power consumption of the sensors, the average power consumption of the system (sensor and interface) is kept as low as 1 μW from a 5 V power supply (with a magnetic field sampling frequency of 1 Hz). The block diagram of the integrated magnetodosimeter is shown in Fig. 13. The system is based on three magnetic sensors which detect the *x, y* and *z* components of the magnetic field $\vec{B} = (B_x, B_y, B_z)$. The current signals produced by the sensors are multiplexed, transformed into voltages, equalized and converted into the digital domain using a single A/D converter. The resulting words representing B_x, B_y and B_z are delivered to the digital section, which calculates the module of the vector and stores the histogram of the magnetic field intensity during the monitored period into a RAM.

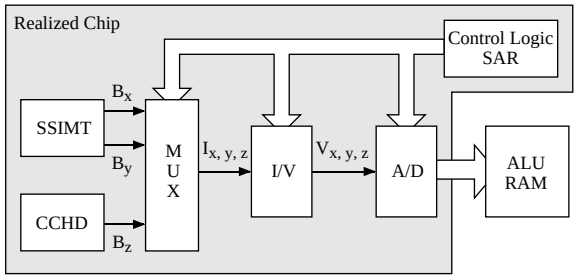

Fig. 13. Block diagram of the integrated magnetodosimeter

The magnetic sensor used to detect B_x and B_y is a quad-collector lateral magnetotransistor with suppressed sidewall injection (SSIMT). In order to detect magnetic fields in the mT range, this device requires an emitter current of a few mA [9]. Fig. 14 illustrates the basic structure and the operating principle of a CMOS-compatible SSIMT (only two collectors are shown for simplicity). In the presence of a magnetic field parallel to the chip plane, the carrier deflection, due to the Lorentz force, enhances the current in one collector at the expense of the other. The resulting differences between the collector currents ($\Delta I_{C1,\,2}$ and $\Delta I_{C3,\,4}$) are proportional to the corresponding components of the magnetic field (B_x and B_y).

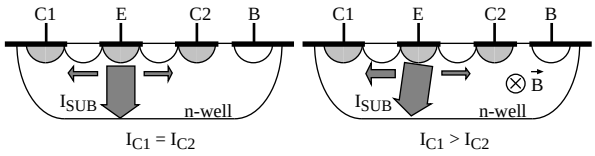

Fig. 14. Operating principle of a CMOS SSIMT

To detect the *z*-component of the magnetic field, we used a CMOS compatible current-controlled Hall device (CCHD) with one input and three output terminals [10]. The layout and the cross-section of this device are shown in Fig. 15. In order to operate the CCHD with sensitivity in the mT range, a fixed current (I_{TOT}) of a few mA is applied to the input terminal (S_{TOT}). Moreover, with a second current source, we control the current $I_0 < I_{TOT}$ extracted from the central output terminal (S_0). Without an external magnetic field, the residual current $I_{1+2} = I_{TOT} - I_0$ is equally divided between the two outer output terminals (S_1 and S_2). In the presence of a magnetic field (B_z) perpendicular to the chip plane, the current in the n-well is deflected due to the Lorentz force acting on the electrons. This leads to a current difference ΔI between S_1 and S_2 proportional to B_z. Since the sensitivity of the CCHD depends on the ratio between I_{TOT} and I_0, we can easily equalize the output signals delivered by the SSIMT and the CCHD, thus allowing a correct detection of the magnetic field module.

In light of the large current required to operate the magnetic sensors (4 to 6 mA), we have to keep the sensors active only during a fraction of the acquisition cycle in order to fulfill the power consumption specifications. It is therefore necessary to use a low power sampling A/D converter, such as the successive approximation architecture with two-step DAC shown in Fig. 16 [11].

This solution consists of a 5-bit resistive DAC for MSB conversion, a 6-bit binary-weighted capacitive DAC for

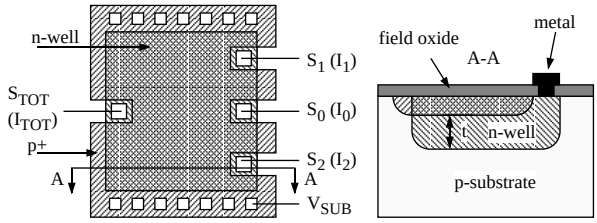

Fig. 15. Layout and cross-section of the CMOS CCHD

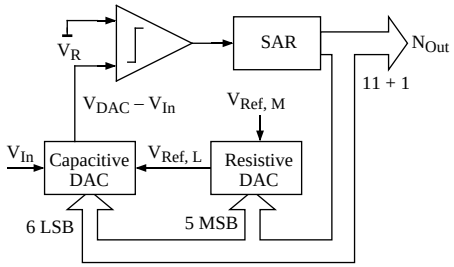

Fig. 16. Block diagram of the successive approximation A/D converter

LSB conversion, a comparator and a Successive Approximation Register (SAR). In this converter, the input signal is sampled and stored in a capacitive array (the capacitive DAC) at the beginning of each conversion cycle, thus allowing to keep the sensors active only for a few tens of µs. Moreover, since this solution requires only 13 clock cycles per conversion (with clock frequency f_{ck} up to 500 kHz), the delay among the three components of the magnetic field due to multiplexed operation is negligible compared to the bandwidth of the considered signals. The resolution achievable with this approach is, of course, determined by resistor and capacitor matching. In this particular case, 12 bit and 6 bit matching are required in the resistive string (MSBs) and in the capacitive array (LSBs), respectively.
The proposed system has been integrated in a standard 0.8 µm CMOS technology. A microphotograph of the chip is shown in Fig. 17, while the measured differential nonlinearity is shown in Fig. 18.

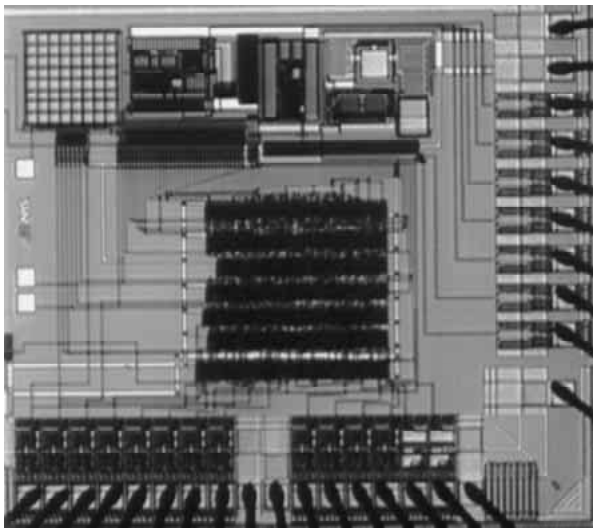

Fig. 17. Microphotograph of the integrated magnetodosimeter

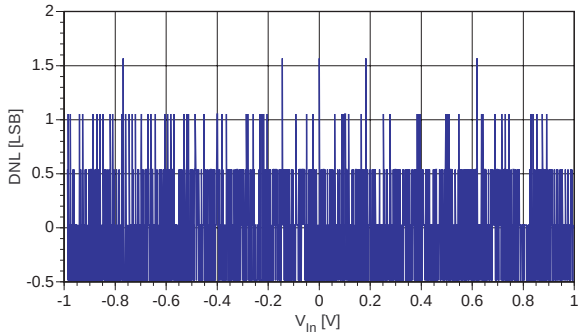

Fig. 18. Measured differential nonlinearity of the successive approximation A/D converter

Sigma-Delta ADC (Humidity Sensor)

The deposition of materials after a conventional CMOS process allows us to sense physical or chemical quantities. For humidity the variation of the dielectric constant in polyimide layers is normally exploited. Fig. 19 shows the structure of a humidity sensor compatible with a conventional CMOS technology [12]. It is made of two interdigitated aluminum electrodes covered by a polyimide layer (or most frequently a layer of material sensitive to a particular chemical). They realize a capacitor whose value, using minimum size elements and area below 0.01 mm^2, is in the range of a fraction of pF. A variation of a few percentage points of the relative humidity causes the capacitance to change by a few tens of aF. Such a variation can be measured by using the switched-capacitor technique or, if digital output is required, by embedding the sensor in a switched capacitor sigma delta modulator [13, 14].

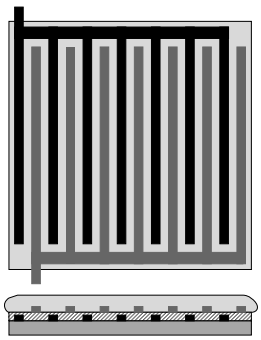

Fig. 19. Humidity sensing capacitor

The schematic of the switched-capacitor, fully-differential second order ΣΔ modulator for capacitive sensor readout is shown in Fig. 20. Capacitor C_S is the humidity sensor while C_R is a reference element, based on the same structure used for C_S but not covered with polyimide. Since C_R is equal to the nominal value of C_S, the circuit only measures the capacitance variation. Voltages V_S and V_R set the sensitivity of the system to humidity and compensate the residual offset of the humidity sensor. The reference voltage V_{Ref} sets the full-scale signal for the humidity measurement.
A microphotograph of the humidity sensing microsystem is shown in Fig. 21, while the digital output of the system as a function of relative humidity is plotted in Fig. 22.

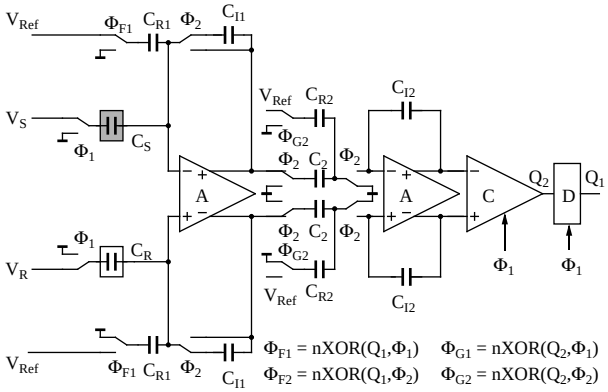

Fig. 20. Schematic of the second order $\Sigma\Delta$ modulator

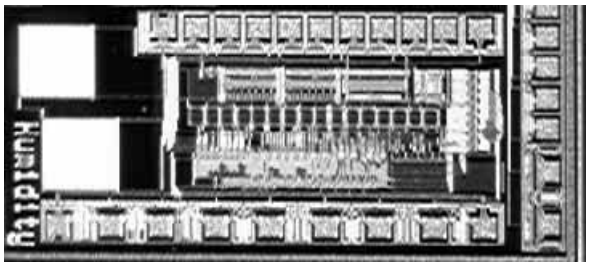

Fig. 21. Microphotograph of the humidity sensor microsystem chip

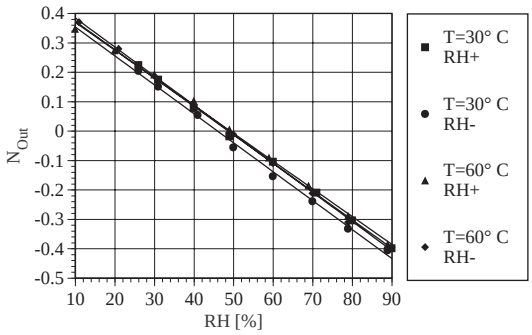

Fig. 22. Digital output of the humidity sensor microsystem

4. Signal Processing

When sensor signals are converted into the digital domain, conventional digital signal processing techniques can be used to perform the required signal conditioning. However, for particular situations, specific signal processing techniques can help in solving detection and recognition problems.

Filtering (Optical IR Sensor)

Nowadays the regulations and the requirements concerning security in domestic and industrial apparates are becoming more stringent and severe. In particular gas and oil burners require necessarily flame monitoring systems, in order to detect the presence of the flame and avoid dangerous leakages of gas or oil [15]. Very simple and cheap ionization probes are typically used in gas burners, in view of the relatively clean environment. These sensors, however, degrade very quickly in oil burners because of the dirt combustion residues. Other available flame detectors placed inside the furnace of oil burners, including thermocouples, microphones and video cameras, provide a low signal-to-noise ratio and easily degrade in the hostile furnace ambient. By contrast, flame monitors based on radiation detection can be placed outside the furnace, in a less harsh and polluted environment, thus increasing significantly long-term stability and reliability of the system.

In particular, silicon IR sensors (photodiodes) can be fabricated using the standard CMOS layers, thus allowing the integration of complex signal processing functions on the sensor chip at very low cost. Of course, in the IR region of the spectrum (from 800 nm to 1000 nm), the emission intensity of the flame is at least one order of magnitude lower than the emission intensity of the furnace. The IR radiation power produced by the furnace, however, is concentrated at DC (or at least at very low frequency), while the unavoidable flickering of the flame spreads the IR radiation power of the burning oil in a frequency band ranging from 50 Hz to 250 Hz. It is, therefore, possible to detect the presence of the flame with a large signal-to-noise ratio by monitoring the IR radiation in this frequency band, while suppressing the large DC component. Thanks to the CMOS compatibility of IR photodiodes, the additional hardware required to perform the filtering can be integrated on the sensor chip, thus making the resulting microsystem very convenient in terms of cost and performance.

The cross-section of a CMOS compatible IR photodiode is shown in Fig. 23. The active junction of the diode (*n*-well/*p*-substrate) is sufficiently deep to allow the generation of electron/hole pairs due to IR radiation.

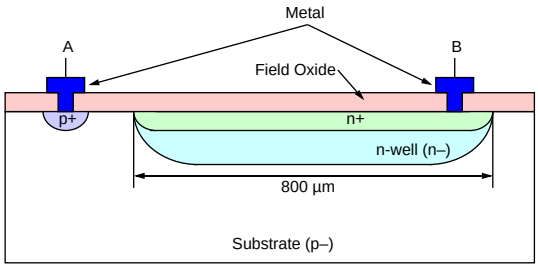

Fig. 23. Cross-section of the CMOS integrated photodiode

The block diagram of the IR flame detector is shown in Fig. 24 [16]. The system consists of an integrated inversely biased IR photodiode, a readout circuit, an analog-to-digital converter (ADC), the digital filters, a digital signal processing circuit and a feedback loop with digital-to-analog converter (DAC) for suppressing the DC component of the IR signal.

The readout circuit for the integrated photodiode has two main functions: provide a suitable biasing voltage for the diode and transform the diode current into a voltage. Both of these tasks are accomplished by an operational amplifier with resistive feedback. The used operational amplifier is based on a standard two-stage class AB structure. The feedback resistor R and the biasing voltage V_B are external, in order to allow sensitivity and operating point adjustments.

The current generated by the photodiode, transformed into a voltage and amplified, is converted into the digital domain by an 8-bit resistor string based successive approximation

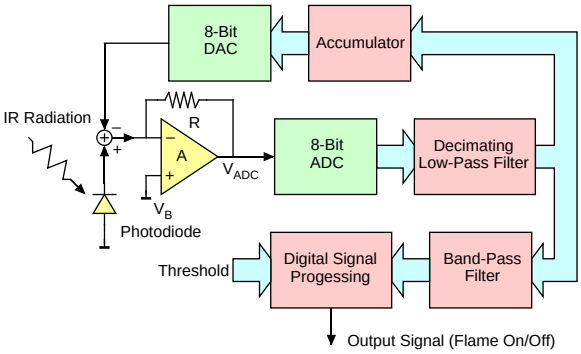

Fig. 24. Block diagram of the infrared radiation detector

ADC with sampling frequency F_{SH} = 32 kHz. The resulting digital word is then down-sampled (decimated) with F_{SL} = 1 kHz, in order to reduce the complexity of the subsequent digital filtering section. The output word of the decimator is delivered either to the feedback loop and to a digital band-pass filter. The feedback loop extracts the DC component of the signal with a digital accumulator and subtracts it directly from the sensor signal by means of an 8-bit current mode DAC (binary weighted current sources). At the same time, the band-pass filtered signal is delivered to the digital signal processor, where it is rectified, accumulated and compared with a programmable threshold, in order to produce an output bit representing the status of the flame. The proposed integrated IR detector has been integrated in a standard 0.8 µm double-poly, double-metal CMOS process. The microphotograph of the chip is shown in Fig. 25. The total die area, including pads is 3.7 mm × 2.5 mm, while the IR photodiode area is 800 µm × 800 µm.

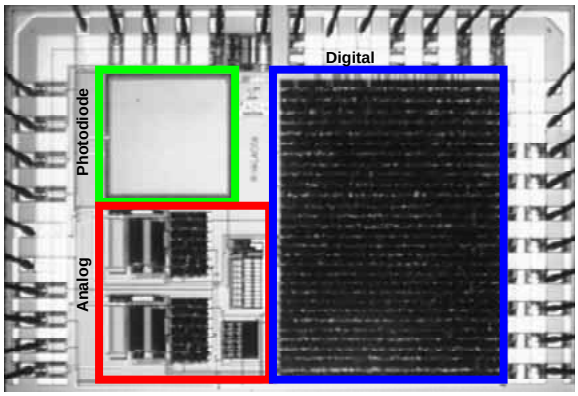

Fig. 25. Microphotograph of the infrared detector chip, including the photodiode, the analog readout circuit and a digital section

Fig. 26 shows the measured transient behavior of the system digital output (*Output*) and of the operational amplifier output voltage (V_{ADC}) when the flame is turned off. To perform this measurement, the flame has been emulated with an IR diode operated at 50 Hz.

Bitstream Processing (Gas Sensor)

A carbon monoxide (CO) gas sensor can be fabricated with a SnO_2 film deposited on a thin membrane realized on a silicon substrate using the bulk-micromachining technique, as shown in Fig. 27. The SnO_2 sensing layer shows a variation in resistance when gases are present.

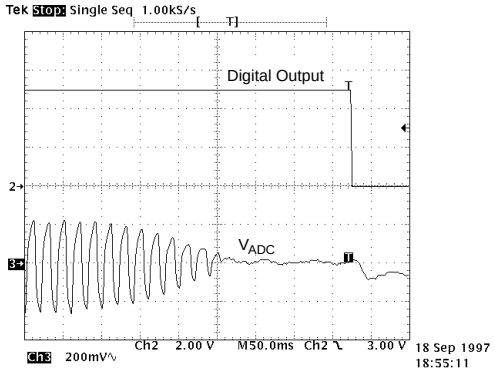

Fig. 26. Measured digital output of the system (Output) and output voltage of the operational amplifier (V_{ADC}) when the flame (emulated with a diode) is turned off

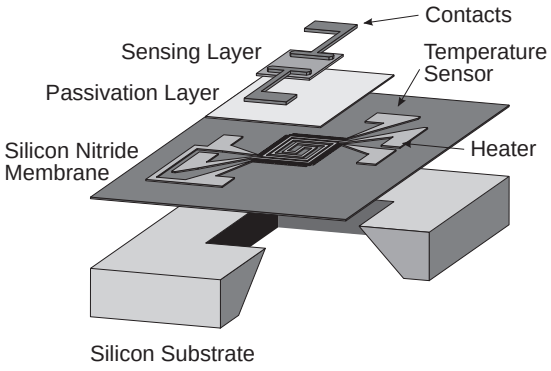

Fig. 27. Carbon monoxide sensor

However, a number of interfering substances (alcohol, methane, air relative humidity) also perturb the sensor conductance. In order to detect only CO concentration, we considered three input signals for the system, namely carbon monoxide (CO), alcohol (C_2H_5OH) and relative humidity (RH), detected by three different sensors. Using a linear model, the three sensor output signals can be expressed as

$$\begin{cases} x_1 = a_1[\mathrm{CO}] + b_1[\mathrm{C_2H_5OH}] + c_1[\mathrm{RH}] \\ x_2 = a_2[\mathrm{CO}] + b_2[\mathrm{C_2H_5OH}] + c_2[\mathrm{RH}] \\ x_3 = c_3[\mathrm{RH}] \end{cases}, \qquad (2)$$

where square brackets denote the gas concentrations. By solving the linear system we can determine the CO concentration independently of other interfering gasses.

This specific signal processing function is performed using sigma-delta bitstreams. The multiplication by a fixed coefficient (between 0 and 1) results from chopping the input of a sigma-delta modulator with a bitstream generated from the coefficient itself, while the addition is realized by interleaving two sigma-delta bitstreams [17].

Since the CO sensor output is actually a resistance variation, we used the sensor itself as input element for a continuous-time sigma-delta modulator, as shown in Fig. 28. The autozero technique is used to cancel the offset and the low frequency noise components.

The fabricated CO sensing system, whose block diagram is shown in Fig. 29 [18], exploits all of these functions to solve Eqn. (2), with respect to CO concentration [19].

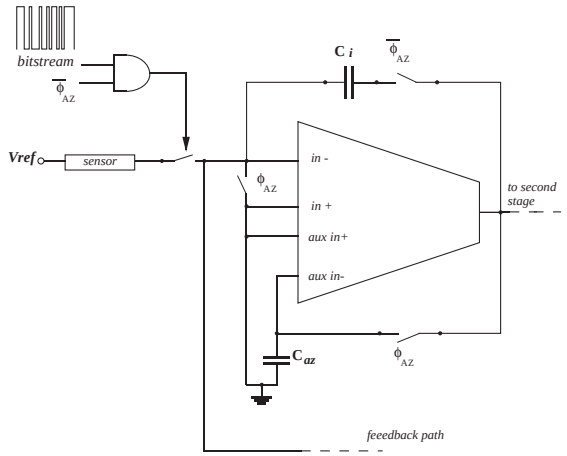

Fig. 28. Schematic of the input stage of the CO sensing system

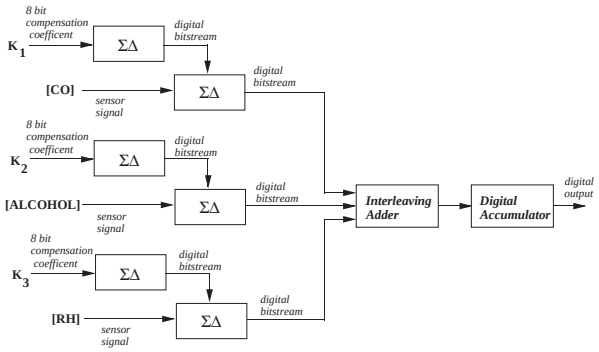

Fig. 29. Block diagram of the CO sensing system

The bitstream processing approach for CO sensing, based on a linearized and simplified model of the sensor response, is suitable to detect the threshold of 150 ppm of CO, required in domestic safety applications.

Acknowledgment

The present work is the result of a long and close cooperation with the Physical Electrical Laboratory, ETH, Zurich, headed by Prof. H. Baltes.

References

[1] H. Baltes, "CMOS as Sensor Technology", *Sensors and Actuators A*, 37-38, pp. 51-56, 1993.

[2] S. Middelhock and S. A. Audet, *Silicon Sensors*, Academic Press, London, 1989.

[3] H. Baltes, O. Paul, J. G. Korvink, M. Schmeider, J. Bühler, N. Schneeberger, D. Jaeggi, P. Malcovati, M. Hornung, A. Häberli, M. von Arx, F. Mayer and J. Funk, "IC MEMS Microtransducers", *IEDM '96 Technical Digest*, San Francisco, CA, pp. 521-524, 1996.

[4] D. Bolliger, R. S. Popovic and H. Baltes, "Integration of a Smart Selective UV Detector", *Tranducers '95 Digest of Technical Papers*, Stockholm, Sweden, pp. 144-147, 1995.

[5] D. Bolliger, P. Malcovati, A. Häberli, P. Sarro, F. Maloberti and H. Baltes, "Integrated Ultraviolet Sensor System with On-Chip 1 GW Transimpedence Amplifier", *ISSCC '96 Digest of Technical Papers*, San Francisco, CA, pp. 328-329, 1996.

[6] R. Lenggenhager and H. Baltes, "Improved Thermoelectric Infrared Sensor Using Double Poly CMOS Technology", *Tranducers'93 Digest of Technical Papers*, Yokohama, Japan, 1993.

[7] P. Malcovati, C. Azeredo Leme, R. Lenggenhager, F. Maloberti and H. Baltes, "Low Noise Multirate SC Read-Out Circuitry for Thermoelectric Integrated Infrared Sensors", *IEEE Trans. Instrumentation and Measurement*, Vol. 44, pp. 795-798, 1995.

[8] A. Häberli, M. Schneider, P. Malcovati, R. Castagnetti, F. Maloberti and H. Baltes, "2D Magnetic Microsensor with On-Chip Signal Processing for Contactless Angle Measurement", , *IEEE J. Solid-State Circuits*, Vol. 31, pp. 1902-1907, 1996.

[9] R. Castagnetti and H. Baltes, "Bipolar Magnetotransistors and Their Trade-Off's", *Sensors and Materials*, Vol. 5, pp. 339-346, 1994.

[10] P. Malcovati, R. Castagnetti, F. Maloberti and H. Baltes, "A Magnetic Sensor with Current Controlled Sensitivity and Resolution", *Sensors and Actuators A*, Vol. 46-47, pp. 284-288, 1995.

[11] P. Malcovati, F. Maloberti, A. Pesucci and M. Poletti, "A 12 Bit A/D interface for 3D Magnetic Sensor", *Proceedings of ISCAS `97*, Hong Kong, pp.1-4, 1997.

[12] T. Boltshauser and H. Baltes, "Capacitive Humidity Sensors in SACMOS Technology with Moisture Absorbing Photosensitive Polyimide", *Sensors and Actuators A*, Vol. 25-27, pp. 509-512, 1990.

[13] P. Malcovati, A. Häberli, F. Mayer, O. Paul, F. Maloberti and H. Baltes, "Combined Air Humidity and Flow CMOS Microsensor with On-Chip 15 Bit Sigma-Delta A/D Interface", *VLSI Circuit Symposium '95 Digest of Technical Papers*, pp. 45-46, 1995.

[14] P. Malcovati, *CMOS Thermoelectric Sensor Interfaces*, Ph. D. Thesis, No. 11424, ETH Zurich, Zurich, Switzerland, 1996.

[15] A. Jones, "Flame Failure Detection and Modern Boilers", J. *Phys. E: Sci. Instrum.*, vol. 21, pp. 921-928, 1988.

[16] P. Bendiscioli, F. Francesconi, P. Malcovati, F. Maloberti, M. Poletti and R. Valacca, "A CMOS Integrated Infrared Radiation Detector for Flame Monitoring", *Proceedings of ISCAS `98*, Monterey, CA, in press.

[17] V. Liberali, P. Malcovati and F. Maloberti, "Sigma-Delta Modulation and Bit-Stream Processing for Sensor Interfaces", *Proceedings of Italian Conference on Sensors and Microsystems*, Rome, Italy, pp. 369-373, 1996.

[18] G. C. Cardinali, L. Dori, M. Fiorini, I. Sayago, G. Faglia, C. Perego, G. Sberveglieri, V. Liberali, F. Maloberti and D. Tonietto, "A smart sensor system for carbon monoxide detection", *Journal of Analog Integrated Circuits and Signal Processing*, vol. 14, pp. 275-296, 1997.

[19] V. Liberali, F. Maloberti and D. Tonietto, "Sigma-Delta Processing in Multisensor Systems for Carbon Monoxide Detection", *Proceedings of ISCAS `98*, vol. 4, Atlanta, GA, pp. 376-379, 1996.